ISSN 1330-3651 (Print), ISSN 1848-6339 (Online)
https://doi.org/10.17559/TV-20220717232926
Original scientific paper

Temperature Distribution and Specific Absorption Rate inside a Child's Eyes from Mobile Phone

Vladimir STANKOVIĆ*, Dejan JOVANOVIĆ, Milan BLAGOJEVIĆ, Miomir RAOS, Anđela JEVTIĆ

Abstract: This paper represents the numerical analysis of Specific Absorption Rate (SAR) and temperature distribution within the eyes of realistic child head model exposed to mobile phone radiation at the frequency of 4G. The SAR and temperature distribution are obtained by numerical solutions of the equation of electromagnetic wave propagation as well as the bioheat equation. The values of SAR and temperature distribution are shown for different biological tissues of the eyes during exposure to electromagnetic radiation from a mobile phone. As electromagnetic properties of tissues depend on the electromagnetic waves' frequency, the value of SAR and temperature will be different for different tissues. For the purpose of this research, a realistic 3D model of a child's head has been created. Maximum absorption of electromagnetic energy occurs in the surface layers of the child head model, whereby this value exceeds the maximum allowed limits. This is the case when the radiation source is positioned closest to the head model. An increase in temperature was observed in the biological tissues and organs closest to the radiation source, i.e. the mobile phone. As the distance between the mobile phone and the child head increases, the temperature decreases, but slower than the SAR values.

Keywords: biological tissue; mobile phone; numerical models; specific absorption rate; temperature change

1 INTRODUCTION

One of the most prominent modes of smart phone use among children is Internet surfing. New functions available on smart phones, such as social network applications with online content sharing, and text and video messaging and chatting propel children to start using smart phones from a very early age.

One thing in common for the majority of phone users is that they hold it directly in front of the face, so that they are able to see the content on the screen better. In this way, phone radiation is directed toward the face and the eyes. Specifically, the eyes of phone users require additional protection not only because they are sensitive organs but also because they are directly exposed to external influences, as the eyelids are their only physical protection.

The eye does not have a regular spherical shape. Adult eye dimensions may differ by only one or two millimetres. The diameter of the adult eye is approximately 24 mm, while at birth it is about 16 - 17 mm. The eyeball grows fast, reaching 22,5 - 23 mm by age three. From age three to 13, the eye reaches its full size. The eye volume is 6,5 ml, while its weight is 7,5 g [1, 2].

Since the eyelids, being the only physical protection of the eyes, are raised while a person is watching the content on the phone screen and since eye moistening is reduced owing to lower frequency of eyelid closure, the eye is directly exposed to the electromagnetic (EM) wave from the phone antenna. Direct exposure of children's eyes to EM radiation from mobile phones causes concern due to potential health issues. Numerous studies have led to the adoption of safety measures prescribing the maximum allowed values of exposure to EM fields [3, 4]. In 2011, the International Agency for Research on Cancer (IARC) classified mobile phone radiation as Group 2B carcinogen based on the evidence indicating higher risk of glioma, a malignant brain cancer, and recommended that further intensive research be conducted [5].

Most studies examining the impact of EM radiation from mobile devices such as tablets, phones, etc. aimed to determine the absorbed energy in standard models of adults [6, 7]. Likewise, the majority of previous studies used a 2D human eye model and a plane wave as the EM radiation source [8, 9]. However, some studies used a 3D model of the human eye to examine the impact of EM radiation from mobile phones and other mobile devices [10, 11].

One study examined the non-thermal effects of high-frequency EM fields on the crystalline lens and found specific damage to the lens epithelium from non-thermal effects, which differed from the damage caused by thermal effects. It was shown that optical quality deterioration of the lens is reversible but that microwaves cause irreversible damage to the epithelial cells of the lens [12].

Another study of the biological effects of mobile phones at 900 MHz indicated that reactive oxygen species (ROS) can play a significant role in retinal oxidative stress [13].

Several studies focused on the effects of mobile phone EM radiation on the lens, the cornea, and the retinal cells [14, 15].

A study investigating the effects of mobile phone radiation at 1800 MHz showed that radiation exposure of no more than 15 minutes twice a day caused retinal disorders in a chick embryo [14]. A different study investigating the effects of mobile phone EM radiation at 900 MHz established the occurrence of oxidative stress in corneal and lens tissues [16]. The study measured the levels of malondialdehyde (MDA) and the activity of superoxide dismutase (SOD), glutathione peroxidase (GSH-Px), and catalase (CAT) in these tissues. The resulting values indicated the presence of oxidative stress.

One study described the influence of EM field on lens clouding and shrinkage or damage of ocular tissues due to reduced blood flow in the human eye [17].

This paper discusses the impact of EM radiation from a mobile phone when it is located directly in front of a child's face. The anatomic shape of the eye model and its properties have a crucial role in the absorption of EM energy, as do the operating frequency and the distance from the EM radiation source.

EM radiation impact assessment is performed based on the obtained results for the amount of absorbed EM energy and the eye tissue temperature change.

2 NUMERICAL METHOD AND MODELING

The Computer Simulation Technology (CST) software package was used to create numerical models of a child's head and eyes and to simulate mobile phone radiation [18].

2.1 Numerical Models

The source of EM radiation is represented by a numerical model of a smart phone [19, 20] containing the casing, the display, and the antenna (Fig. 1). The antenna was modelled for the frequency of 0,8 GHz, which is one of the 4G mobile networks, with a reference power of P = 1 W [21] and an impedance of Z = 50 Ω.

Figure 1 Actual smart phone

In order to determine the impact of EM waves on a child's eyes, the amount of energy absorbed, and the temperature increase due to EM wave energy absorption, we designed a numerical model of a child's head [19] and eyes. The properties, dimensions, and anatomical shape of these models correspond to a seven-year-old child. Fig. 2 shows the external appearance of a child head and eyes model. The arbitrary cross-section of the child head model with the layout of tissues/organs is shown in Fig. 3. The numbers in Fig. 3 denote the corresponding tissues presented in Tab. 1 and Tab. 2.

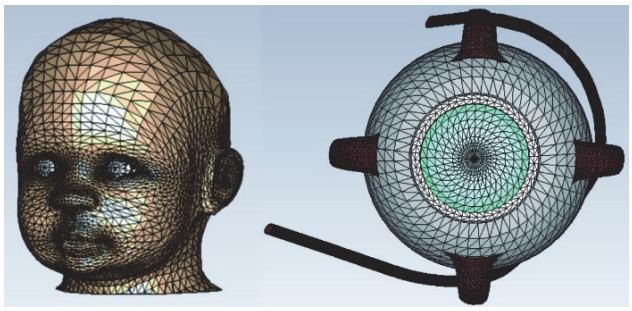

Figure 2 External appearance of the child head and eye models

During the modelling, it is necessary to describe all tissues and organs according to their EM properties. A detailed knowledge of EM properties of biological tissues and organs (permittivity, conductivity, permeability, and density) is essential to understanding the interaction between EM radiation and a specific biological structure. The values of EM properties of tissues and organs for the given frequency are shown in Tab. 1 and Tab. 2 (for the eyes) [22-24].

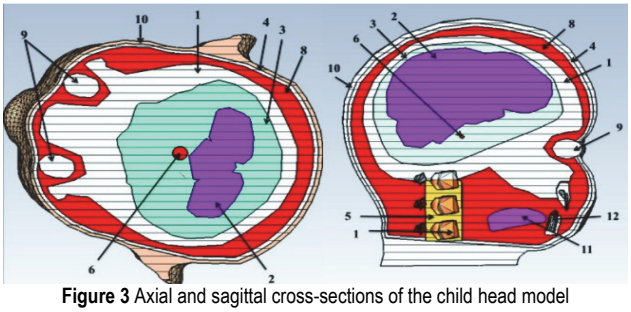

Figure 3 Axial and sagittal cross-sections of the child head model

Table 1 Electromagnetic properties of tissues at 0,8GHz

	Tissues/organs	ε_r	Σ / S/m	ρ / kg/m^3
1.	Cortical Bones	12,6	0,132	1908
2.	Brain	46,3	0,730	1046
3.	Cerebrospinal fluid	68,9	2,370	1007
4.	Fat	11,4	0,102	911
5.	Cartilage	43,0	0,738	1100
6.	Pituitary gland	59,6	1,030	1053
7.	Spinal cord	32,9	0,548	1075
8.	Muscle	55,3	0,910	1090
9.	Eyes (The EM properties are given in Tab. 2.)			
10.	Skin	42,0	0,834	1109
11.	Tongue	55,6	0,900	1090
12.	Teeth	12,6	0,132	2180
13.	Vertebrae	12,6	0,132	1908

The cross-section of the eye with tissue layout is shown in Fig. 4, with the numbers corresponding to those given for the tissues in Tab. 2.

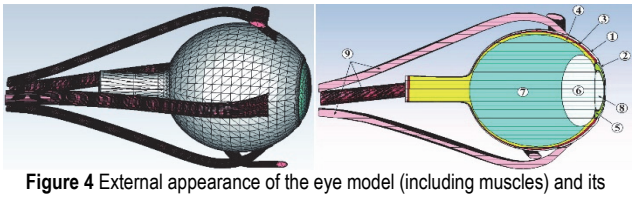

Figure 4 External appearance of the eye model (including muscles) and its cross-section

Table 2 Electromagnetic properties of eye tissues at 0.8GHz

	Tissue	ε_r	σ / S/m	ρ / kg/m^3
1.	Sclera	55,6	1,13	1032
2.	Cornea	55,7	1,35	1051
3.	Choroid	61,7	1,50	1060
4.	Retina	53,3	0,90	1039
5.	Iris	55,3	0,91	1040
6.	Lens	36,0	0,46	1076
7.	Vitreous Body	68,9	1,61	1005
8.	Aqueous Humour	68,9	2,37	1010
9.	Muscle	55,3	0,91	1090

2.2 SAR Calculation

When an EM wave propagates through biological tissue, the tissue absorbs the EM wave energy. The interaction between EM waves and biological tissues can be described by a quantity called Specific Absorption Rate (SAR). SAR is defined as the speed of power dissipation normalized by the density of the material, and it can be expressed by the following equation:

$$\mathrm{SAR} = \frac{\sigma}{\rho}|E|^2 \tag{1}$$

where σ is electrical conductivity (S/m) and ρ is tissue density (kg/m^3). It should also be noted that the electric field E (V/m) is the root mean square value.

In addition, it is very important to define averaged SAR as the ratio of the power absorbed in the tissue and the weight of that biological tissue. The averaged SAR is obtained by the expression:

$$\mathrm{SAR}_{\mathrm{av}} = \frac{1}{V}\int_V \mathrm{SAR}\,\mathrm{d}V = \frac{1}{V}\int_V \frac{\sigma}{\rho}|E|^2\,\mathrm{d}V \tag{2}$$

Mass averaged SAR is typically calculated for a sample of 1 g (SAR_{1g}) and a sample of 10g (SAR_{10g}). In this paper, SAR will be averaged only for 1 g, due to the small volume of an eye.

2.3 Temperature Calculation

As stated, SAR is the basic measurement for assessing the safety of exposure to RF EM radiation prescribed by the standards. However, temperature increase inside the human head is one of the dominant factors of harmful physiological effects. In fact, it has been suggested that a temperature increase of about 3,5 °C in the brain should be the allowed limit that does not cause any physiological damage [25]. Yet, there are also reports that a small temperature increase in the hypothalamus (0,2 - 0,3 °C) alters the thermoregulation behaviour [26].

Knowledge of the thermal properties of biological tissues is the foundation for understanding heat transfer in biological systems. Heat transfer in living tissues is a complex process, which involves the combination of thermal conductivity in tissues, propagation and blood perfusion, and metabolic heat generation. The energy deposed in tissues causes temperature increase, but the temperature also depends on the tissue thermoregulation system. Tissue temperature may continuously increase if the absorbed energy exceeds the metabolic response of the tissue's thermoregulation system, such as blood perfusion.

Temperature distribution in tissues during exposure to EM waves can be determined by solving the bioheat equation, which takes into consideration heat conduction, blood perfusion, and external heating. The temperature distribution in the child's eyes model was obtained by solving Pennes' bioheat equation [27] with the addition of the member $\rho_{\mathrm{tk}}\mathrm{SAR}$, which denotes the volumetric density of absorbed power originating from an external source [28]:

$$\rho_{\mathrm{tk}} C_{\mathrm{tk}} \frac{\partial T_{\mathrm{tk}}}{\partial t} = \nabla . k_{\mathrm{tk}} \nabla T_{\mathrm{tk}} + \rho_{\mathrm{kr}} C_{\mathrm{kr}} \omega_{\mathrm{kr}} \left(T_{\mathrm{art}} - T_{\mathrm{tk}}\right) + \\ + q_{\mathrm{m}} + \rho_{\mathrm{tk}}\mathrm{SAR} \tag{3}$$

where ρ_{tk}, C_{tk}, T_{tk}, and k_{tk} denote density, specific heat, tissue temperature, and thermal tissue conductivity, respectively; T_{art} is arterial blood temperature, ω_{kr} is the blood perfusion rate, ρ_{kr} is blood density, C_{kr} is specific blood heat, and q_{m} is the metabolic heat generation rate in $\mathrm{W/m^3}$.

Tab. 3 shows the thermal parameters of eye tissues [24].The convective heat transfer coefficient between the model surface and the air is set to 5 $\mathrm{W/m^2K}$ [29]. The ambient temperature is set to 25 °C and the blood temperature is set to 37 °C.

Table 3 Thermal parameters of eye tissues

Tissue		k / W/m°C	c / J/kg°C	B / $\mathrm{W/m^3°C}$
1.	Sclera	0,58	3800	80000
2.	Cornea	0,52	3600	0
3.	Choroid	0,58	3800	80000
4.	Retina	0,58	3800	80000
5.	Iris	0,52	3600	35000
6.	Lens	0,40	3000	0
7.	Vitreous Body	0,58	4000	0
8.	Aqueous Humour	0,58	4000	0
9.	Muscle	0,50	3800	2700

3 RESULTS

3.1 SAR Distribution

The simulation considers the impact of mobile phone radiation on child's eyes model for different distances from the front of the face. The phone is placed vertically in front of the child head model, in a position suitable for viewing the screen content at the distances of 3, 6, 9, and 12 cm. Considering the fact that the eye is a small organ weighing less than 10 g, it is unnecessary to analyse the distribution of SAR_{10g}, because the end volume will nevertheless encompass the part of the tissue not belonging to the eye.

Fig. 5 shows the section of the child head model with directions along which the changes of SAR and temperature values were analysed.

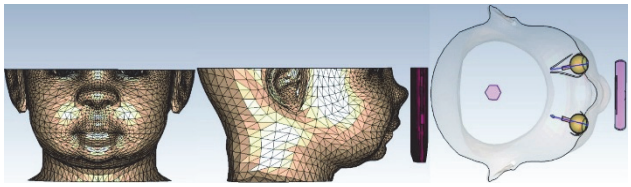

Figure 5 Section of the child head model in the middle of the eyes with drawn analysis directions

Fig. 6 to Fig. 9 show the distribution of SAR_{1g} at the surface of the head model and within the model for the horizontal cross-section in line with the pupils and for different distances from the radiation source.

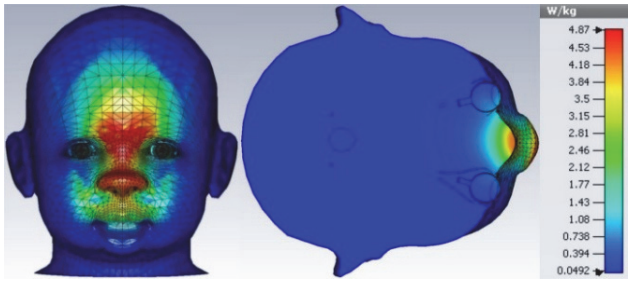

Figure 6 Distribution of SAR_{1g} / W/kg for the child head model's distance of 3 cm from the phone

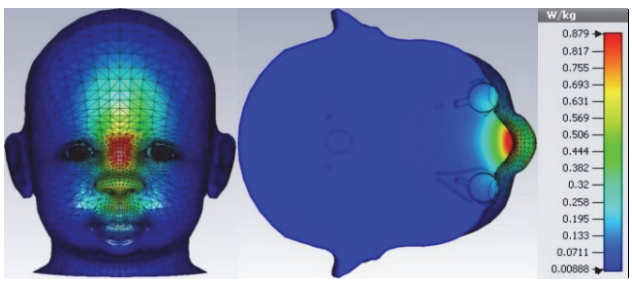

Figure 7 Distribution of SAR_{1g} / W/kg for the child head model's distance of 6 cm from the phone

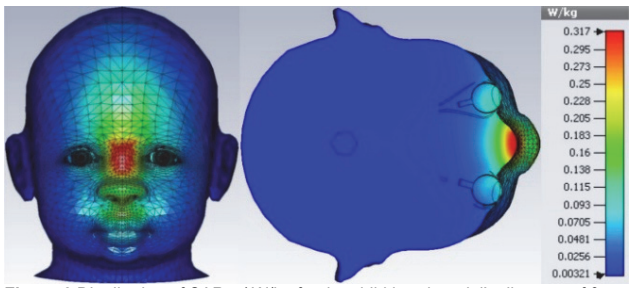

Figure 8 Distribution of SAR_{1g} / W/kg for the child head model's distance of 9 cm from the phone

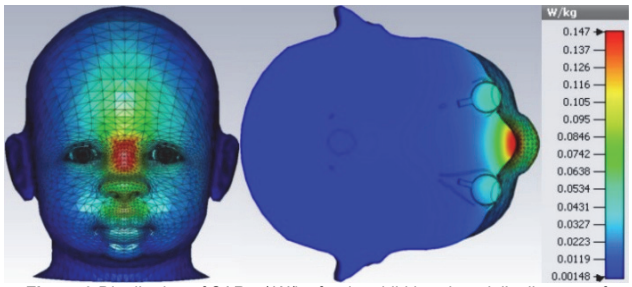

Figure 9 Distribution of SAR_{1g} / W/kg for the child head model's distance of 12 cm from the phone

The largest amount of absorbed energy is concentrated in the front of the face, from the upper lip to the forehead. Fig. 9 shows that the upper part of the nose has the highest values of absorbed energy. The maximum value of SAR_{1g} at the distance of 3 cm is 4,87 W/kg, which is considerably higher (about three times) than the base limit value [3]. High SAR_{1g} values are also observed inside the model, as seen from the cross-section in Fig. 6. For other distances, these values are significantly lower than the base limit.

Fig. 10 and Fig. 11 show the SAR_{1g} dependency on the distance for the right and the left eye, respectively.

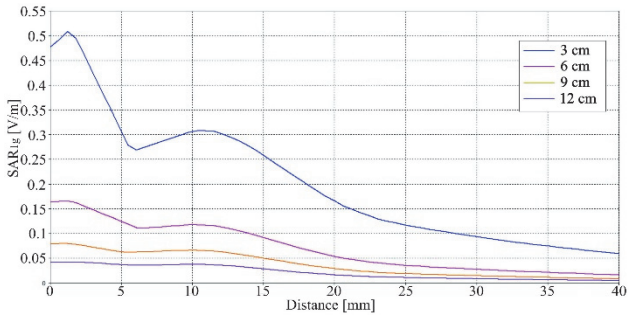

Figure 10 Graph of SAR_{1g} / W/kg distribution for the right eye for all four distances from the phone

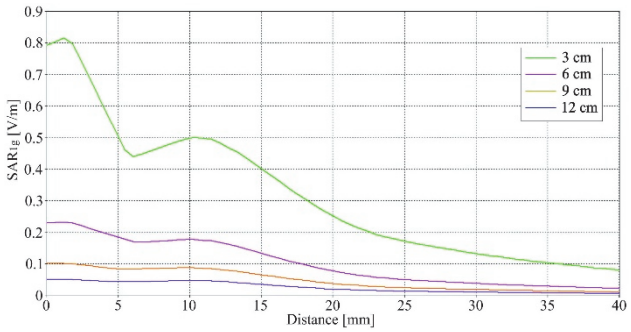

Figure 11 Graph of SAR_{1g} / W/kg distribution for the left eye for all four distances from the phone

The shape of SAR_{1g} distribution graph for the given distances is almost identical for both eyes. The highest SAR_{1g} is registered in the left eye for the distance of 3 cm, amounting to 0,82 W/kg, while the corresponding right eye value is 0,51 W/kg. The values for other distances are considerably lower. A slightly higher SAR_{1g} value is observed in the left eye due to the antenna pattern.

3.2 Temperature Distribution

Fig. 12 to Fig. 15 show the temperature change at the surface of the child head model and for the horizontal cross-section along the middle of the eyes. The initial temperature of 37 °C is set to zero in the colour palette to improve the visibility of temperature changes.

In all cases, the use of a mobile phone is simulated at a constant power of 1 W and for the time period of 30 min. The time that the average user spends reading the content from the phone screen is longer than the time spent talking on the phone. This is why the duration of exposure while reading differs from the duration of phone conversation simulation.

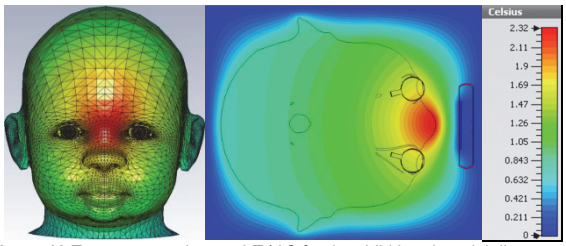

Figure 12 Temperature change ΔT / °C for the child head model distance of 3 cm from the phone

Fig. 12 shows that the maximum temperature increase from the initial temperature is as high as 2,32°C and that the temperature increase does not fall below 1°C in almost two-thirds of the child head model. The highest temperatures are primarily found in the nose skin, the fat tissue, and the skull. Likewise, the eyes are also characterized by significantly increased temperature values.

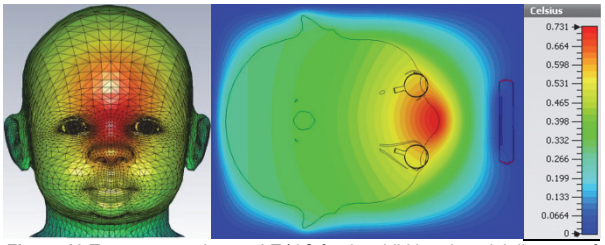

Figure 13 Temperature change ΔT / °C for the child head model distance of 6 cm from the phone

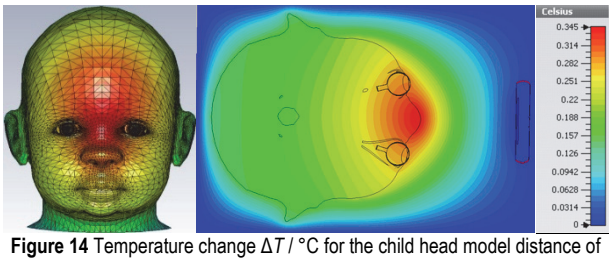

Figure 14 Temperature change ΔT / °C for the child head model distance of 9 cm from the phone

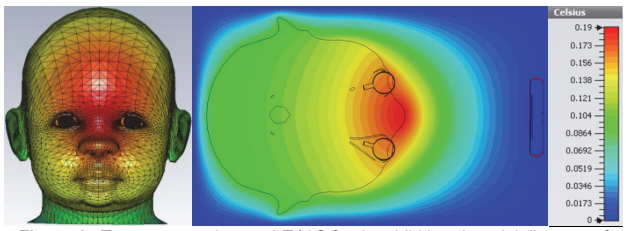

Figure 15 Temperature change ΔT / °C for the child head model distance of 12 cm from the phone

Relatively higher temperature increases 0,73 °C are found for the distance of 6cm, while the values were much lower in other cases, 0,345 °C and 0,19 °C for 9 cm and 12 cm, respectively.

Fig. 16 and Fig. 17 show the curves of temperature change ΔT / °C depending on the distance for the right and the left eye, respectively, along the analysed directions.

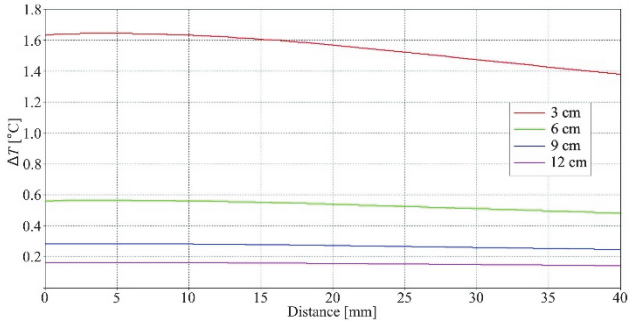

Figure 16 Temperature increase ΔT / °C for the right eye for all four distances

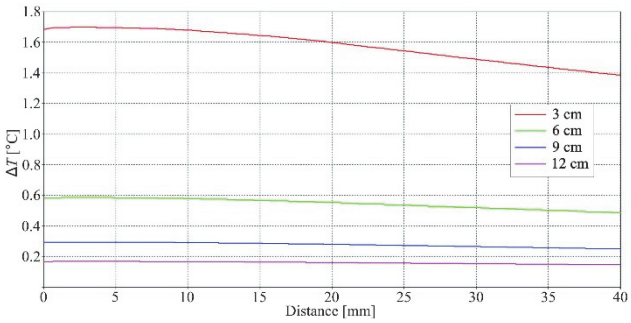

Figure 17 Temperature increase ΔT / °C for the left eye for all four distances

The shape of the temperature change graph dependent on the distance for both eyes is much more uniform than in the case of SAR value changes. Likewise, there is a noticeably smaller difference between the lower and upper limits of temperature change, i.e. temperature distribution is fairly homogeneous.

For the distance of 3 cm, the biggest temperature change in the right eye along the given direction is 1,64 °C, while the smallest is 1,38 °C. The difference in temperature between the front of the eye and the end of the optic nerve is only 0,26 °C, which is about 15,8% lower than the maximum value. For the distance of 6 cm, the biggest change is 0,565 °C at the front of the eye, for 9 cm it is 0,284 °C, and for 12 cm it is 0,162 °C. In all three cases, the difference between the highest and the lowest values is between 12% and 15% on average.

Along the direction of the left eye, the values are slightly higher, so that the biggest change for the 3 cm distance is 1,695 °C, for 6cm it is 0,585 °C, for 9 cm it is 0,293 °C, and for 12 cm it is 0,166 °C. For all distances, the difference between the highest and the lowest values is from 18% to 13% as the distance increases.

4 CONCLUSION

Based on the analysis of the results obtained from the simulations of energy absorption in the child head and eyes model, it can be concluded that the largest amount of absorbed energy was concentrated in the front of the face, from the upper lip to the forehead. The maximum SAR_{1g} value at the distance of 3 cm was considerably (about three times) higher than the base limit value. For other distances between the head model and the phone, these values were significantly lower than the base limit. However, the SAR_{1g} values in the eyes for all four distances from the phone were below the base limit.

With regard to temperature change, significant temperature increase was found in the child's eyes model. As expected, the biggest temperature increase of 2,32 °C was obtained for the highest proximity of the phone to the head. Yet, the increase was not registered in the eyes themselves but between the eyes. For the smallest distance, the biggest temperature increase in the eyes was 1,8 °C, while this value dropped to 0,2 °C for the largest simulated distance.

Significant temperature increase in the surface layers of the model and the eyes was found only when the phone was positioned very close to the face. When the phone was sufficiently far from the face, there was no significant temperature increase in the surface layers of the child's face and eyes.

According to the previous analysis, it can be concluded that the expected SAR values for mobile phone distances from the child's face that are common when viewing phone screen content do not exceed the reference limit levels and the base limits in children's eyes. Similarly, the temperature increase in the eyes does not reach high values for any usual period of phone use. This leads to the conclusion that using the phone in this way is safer than using a mobile phone during a conversation, when it is positioned next to the user's head.

Naturally, with regard to SAR values, it has to be remembered that the front part of the face from the upper lip to the forehead exhibited high SAR_{1g} values at small distances from the radiation source, which were significantly (about three times) higher than the base limit values. A similar conclusion can be drawn for the temperature increase in the same part of the face. Namely, the temperature increase was as much as 2,32 °C higher than the initial value for the smallest analysed distance, while the increase was at least 1°C in almost two-thirds of the child head model.

Acknowledgements

This research was supported by the Ministry of Education, Science and Technological Development of the Republic of Serbia.

5 REFERENCES

[1] http://oci.rs/ljudsko-oko.

[2] Hogan, M. J. (1971). *Histology of the human eye an atlas and text book*. WB Saunders, Michigan.
[3] IEEE (2006). IEEE Standard for safety levels with respect to human exposure to radio frequency electromagnetic fields, 3 kHz to 300 GHz. Inc. C95.1-2005. https://doi.org/10.1109/IEEESTD.2006.99501
[4] https://www.kvalitet.co.rs/dokumenta/zakoni/nejonizujuce/Pravilnik-o-granicama-izlaganja-nejonizujucim-zracenjima.pdf
[5] http://www.iarc.fr/en/media-centre/pr/2011/pdfs/pr208_E.pdf
[6] Bhat, M. A. & Kumar, V. (2013). Calculation of SAR and measurement of temperature change of human head due to the mobile phone waves at frequencies 900 MHz and 1800 MHz. *Adv. Phys. Theor. Appl*., *16*, 54-63.
[7] Wessapan, T., Srisawatdhisukul, S., & Rattanadecho, P. (2012). Specific absorption rate and temperature distributions in human head subjected to mobile phone radiation at different frequencies. *Int. J. Heat Mass Transf.*, *55*, 347-359. https://doi.org/10.1016/j.ijheatmasstransfer.2011.09.027
[8] Wessapan, T. & Rattanadecho, P. (2013). Specific absorption rate and temperature increase in the human eye due to electromagnetic fields exposure at different frequencies. *Int. J. Heat Mass Transfer*, 64, 426-435. https://doi.org/10.1016/j.ijheatmasstransfer.2013.04.060
[9] Hirata, A. (2005). Temperature increase in human eyes due to near-field and far-field exposures at 900 MHz, 1.5 GHz, and 1.9 GHz. *IEEE Trans. Electromagn. Compat.*, 47, 68-76. https://doi.org/10.1109/TEMC.2004.842113
[10] Schaumburg, F. & Guarnieri, F. A. (2017). Assessment of thermal effects in a model of the human head implanted with a wireless active microvalve for the treatment of glaucoma creating a filtering bleb. *Phys. Med. Biol.*, *62*(9), 191-203. https://doi.org/10.1088/1361-6560/aa5dae
[11] Cvetković, N., Krstić, D., Stanković, V., & Jovanović, D. (2018). Electric field distribution and SAR inside a human eye exposed to VR glasses. *IETMicrow. Antennas Propag.*, *12*(14), 2234-2240. https://doi.org/10.1049/iet-map.2018.5227
[12] Dovrat, A., Berenson, R., Bormusov, E., Lahav, A., Lustman, T. Sharon, N., & Schachter, L. (2005). Localized effects of microwave radiation on the intact eye lens in culture conditions. *Bio electro magnetics*, *26*, 398-405. https://doi.org/10.1002/bem.20114
[13] Ozguner, F., Bardak, Y., & Comlekci, S. (2006). Protective effects of melatonin and caffeic acid phenethyl ester against retinal oxidative stress in long-term use of mobile phone: a comparative study. *Mol Cell Biochem*, *282*, 83-88. https://doi.org/10.1007/s11010-006-1267-0
[14] Zareen, N., Khan, M. Y., & Ali Minhas, L. (2009). Derangement of chick embryo retinal differentiation caused by radiofrequency electromagnetic fields. *Congenit Anom*, *49*, 15-19. https://doi.org/10.1111/j.1741-4520.2008.00214.x
[15] Siegfried, C. J., Shui, Y. B., Holekamp, N. M., Bai, F., & Beebe, D. C. (2011). Racial differences in ocular oxidative metabolism: implications for ocular disease. *Arch Ophthalmol*, *129*, 849-854. https://doi.org/10.1001/archophthalmol.2011.169
[16] Balci, M., Devrim, E., & Durak, I. (2007). Effects of mobile phones on oxidant/antioxidant balance in cornea and lens of rats. *Curr Eye Res*, *32*, 21-25. https://doi.org/10.1080/02713680601114948
[17] Mirnezami, S. A., Jafarabadi, M. R., & Abrishami, M. (2013). Temperature distribution simulation of the human eye exposed to laser radiation. *Journal of Lasers in Medical Sciences*, *4*(4), 175-181.
[18] www.cst.com.
[19] Stanković, V., Jovanović, D., Krstić, D., Marković, V., & Cvetković, N. (2017). Temperature distribution and specific absorption rate inside a child's head. *International Journal of Heat and Mass Transfer*, *104*, 559-565. https://doi.org/10.1016/j.ijheatmasstransfer.2016.08.094
[20] Jovanovic, D. B., Stankovic, V., Cvetkovic, N. N., Krstic, D., & Vuckovic, D. (2019). The impact of human age on the amount of absorbed energy from mobile phone. *COMPEL*, *38*(5), 1465-1479. https://doi.org/10.1108/COMPEL-12-2018-0511
[21] C95.3-2002 IEEE Recommended Practice for Measurements and Computations of Radio Frequency Electromagnetic Fields with Respect to Human Exposure to Such Fields, 100 kHz - 300 GHz. https://doi.org/10.1109/IEEESTD.2002.94226
[22] http://www.itis.ethz.ch/itis-for-health/tissue-properties/database/dielectric-properties/
[23] Gabriel, C. (1996). *Compilation of the dielectric properties of body tissues at RF and microwave frequencies*. King's College London. https://doi.org/10.21236/ADA303903
[24] Hirata, A., Watanabe, S., Fujiwara, O., Kojima, M., Sasaki, K., & Shiozawa, T. (2007). Temperature elevation in the eye of anatomically based human head models for plane-wave exposures. *Phys. Med. Biol.*, *52*(21), 6389-99. https://doi.org/10.1088/0031-9155/52/21/003
[25] Guyton, A. C. & Hall, J. E. (1996). *Medical Physiology*, Saunders, Philadelphia, PA, Ch. 73.
[26] Adair, E. R., Adams, B. W., & Akel, G. M. (1984). Minimal changes in hypothalamic temperature accompany microwave-induced alteration of thermoregulatory behaviour. *Bio electro magnetics*, *5*(1), 13-30. https://doi.org/10.1002/bem.2250050103
[27] Zolfaghari, A. & Maerefat, M. (2011). Bioheat Transfer. *Developments in Heat Transfer*. https://doi.org/10.5772/22616
[28] Carluccio, G., Oh, S., & Collins, C. M. (2011). Ultra-Fast Calculation of SAR-induced Temperature Increase. *Proc. Intl. Soc. Mag. Reson. Med.*, *19*, 38-44.
[29] Fiala, D., Lomas, K. J., & Stohrer, M. (1999). A computer model of human thermoregulation for a wide range of environmental conditions: the passive system. *J. Appl. Physiol*., 87, 1957-1972. https://doi.org/10.1152/jappl.1999.87.5.1957

Contact information:

Vladimir STANKOVIĆ, PhD, Assistant Professor
(Corresponding author)
University of Niš, Faculty of Occupational Safety,
Čarnojevića 10a, 18000 Niš, Serbia
E-mail: vladimir.stankovic@znrfak.ni.ac.rs

Dejan JOVANOVIĆ, PhD, Teaching Assistant
University of Niš, Faculty of Electronic Engineering,
A. Medvedeva 14, 18000 Niš, Serbia
E-mail: dejan.jovanovic@elfak.ni.ac.rs

Milan BLAGOJEVIĆ, PhD, Full Professor
University of Niš, Faculty of Occupational Safety,
Čarnojevića 10a, 18000 Niš, Serbia
E-mail: milan.blagojevic@znrfak.ni.ac.rs

Miomir RAOS, PhD, Full Professor
University of Niš, Faculty of Occupational Safety,
Čarnojevića 10a, 18000 Niš, Serbia
E-mail: miomir.raos@znrfak.ni.ac.rs

Anđela JEVTIĆ, MSc student, Student demonstrator
University of Niš, Faculty of Occupational Safety,
Čarnojevića 10a, 18000 Niš, Serbia
E-mail: andjela.jevtic@znrfak.ni.ac.rs